

The Summer North Atlantic Oscillation: Past, Present, and Future

CHRIS K. FOLLAND AND JEFF KNIGHT

Met Office Hadley Centre, Exeter, Devon, United Kingdom

HANS W. LINDERHOLM

Department of Earth Sciences, University of Gothenburg, Gothenburg, Sweden

DAVID FEREDAY AND SARAH INESON

Met Office Hadley Centre, Exeter, Devon, United Kingdom

JAMES W. HURRELL

National Center for Atmospheric Research, Boulder, Colorado

(Manuscript received 31 January 2008, in final form 26 August 2008)

ABSTRACT

Summer climate in the North Atlantic–European sector possesses a principal pattern of year-to-year variability that is the parallel to the well-known North Atlantic Oscillation in winter. This summer North Atlantic Oscillation (SNAO) is defined here as the first empirical orthogonal function (EOF) of observed summertime extratropical North Atlantic pressure at mean sea level. It is shown to be characterized by a more northerly location and smaller spatial scale than its winter counterpart. The SNAO is also detected by cluster analysis and has a near-equivalent barotropic structure on daily and monthly time scales. Although of lesser amplitude than its wintertime counterpart, the SNAO exerts a strong influence on northern European rainfall, temperature, and cloudiness through changes in the position of the North Atlantic storm track. It is, therefore, of key importance in generating summer climate extremes, including flooding, drought, and heat stress in northwestern Europe. The El Niño–Southern Oscillation (ENSO) phenomenon is known to influence summertime European climate; however, interannual variations of the SNAO are only weakly influenced by ENSO. On interdecadal time scales, both modeling and observational results indicate that SNAO variations are partly related to the Atlantic multidecadal oscillation. It is shown that SNAO variations extend far back in time, as evidenced by reconstructions of SNAO variations back to 1706 using tree-ring records. Very long instrumental records, such as central England temperature, are used to validate the reconstruction. Finally, two climate models are shown to simulate the present-day SNAO and predict a trend toward a more positive index phase in the future under increasing greenhouse gas concentrations. This implies the long-term likelihood of increased summer drought for northwestern Europe.

1. Introduction

Climate variability in the North Atlantic–European sector is strongly governed by variability in atmospheric circulation. This is most true in winter, for which the paradigm of the North Atlantic Oscillation (NAO; see

Walker 1924) has provided a clear framework for many studies of the year-to-year climate variability of the region. There is less recognition, however, of the role of circulation variability in European summer climate, although it has been noted in a number of previous studies, often as an extension of analyses focused on the winter. Thus the eigenvector analyses of North Atlantic–European mean sea level pressure of Hurrell and van Loon (1997), Hurrell and Folland (2002), and Hurrell et al. (2003) do contain a leading pattern of summer circulation variability. In the latter study, this pattern explains 22.1% of

Corresponding author address: Prof. Chris Folland, Met Office Hadley Centre, FitzRoy Road, Exeter, Devon EX1 3PB, United Kingdom.
E-mail: chris.folland@metoffice.gov.uk

June–August (JJA) mean sea level pressure (MSLP) variance in the extratropical North Atlantic compared with 36.7% for the NAO in winter. The summer pattern has a smaller spatial extent than the winter NAO and is located farther north, with the southern node over northwest Europe, rather than the Azores–Spain region, and a smaller-scale Arctic node (Fig. 6 of Hurrell et al. 2003). A similar result appears in the rotated eigenvector analysis of monthly Northern Hemisphere 700-hPa geopotential height of Barnston and Livezey (1987, hereafter BL87). BL87 show almost identical leading patterns in June, July, and August, explaining similar hemispheric variance (10%) to the typical winter monthly NAO (12%). The results of these studies show there is a summertime counterpart to the winter NAO, albeit with different characteristics. By analogy with the winter season, we refer to this pattern of variability as the summer North Atlantic Oscillation (SNAO). Our aim is to more firmly establish the SNAO as a key paradigm in understanding European summer climate variability and to explore its characteristics.

A different approach to characterizing the seasonal cycle of the NAO was developed by Portis et al. (2001) through their concept of the “mobile NAO.” For each month of the year the points of maximum anticorrelation of National Centers for Environmental Prediction (NCEP) reanalysis (Kalnay et al. 1996) MSLP between two regions (55° – 80° N, 70° W– 0° and 20° – 45° N, 70° W– 0°) were computed. In contrast to other studies, for July and August they obtained dipoles with centers in the western North Atlantic. The ranges of longitude and latitude permitted by the anticorrelation calculations, however, prevent the possibility of a more northward and eastward southern node, excluding the SNAO as defined above. It is important, therefore, that variability over the whole North Atlantic region be taken into account in establishing the leading mode of summer variability.

Another method of identifying regional atmospheric circulation patterns is through cluster analysis. Cassou et al. (2005) carried out a *k*-means cluster analysis of daily JJA 500-hPa heights over the North Atlantic–European region (20° – 80° N, 90° W– 30° E). By retaining only the days identified as being in the same cluster for 5 consecutive days or longer, they identified four clusters each explaining about 18% of the variance. One of these patterns (which they call the “summer European blocking pattern”) is similar to the SNAO as it appears in Hurrell and van Loon (1997), Hurrell et al. (2003), or BL87, despite being derived from daily data and a different level of the atmosphere. In their definition of its positive mode, which fits that of the above investigators, high pressure anomalies dominate northern Europe.

Horel (1981) noted a tendency for some 500-hPa teleconnection patterns to possess a smaller meridional scale in Northern Hemisphere summer than in winter, which he partly ascribed to the northward movement of the storm track between winter and summer. Recently, Feldstein (2007) has analyzed the mechanisms of JJA NAO dynamics using the BL87 index. The 300-hPa-level pattern most strongly related to the BL87 index is displaced a little to the west of the BL87 surface pattern. The smaller scale of summer patterns compared to those in winter is also noted. Ogi et al. (2004, 2005) have identified a summer annular mode based on zonally averaged data that parallels the winter annular mode of Thompson and Wallace (1998). This mode also has a smaller meridional scale than the corresponding winter annular mode. The smaller zonal scale of the SNAO compared to the winter NAO makes a relationship with an annular mode less applicable. Nevertheless, Ogi et al. (2004) point out it is likely that a consistent description of modes of extratropical Northern Hemisphere climate through the seasonal cycle demands analyses which are seasonally specific because of seasonal changes in their spatial scale.

In this paper we perform analyses which confirm that the SNAO is a principal mode of climate variability in North Atlantic–European summer. Although it has different characteristics than the wintertime NAO, the SNAO provides a similar paradigm for understanding the year-to-year variations of seasonal climate. We concentrate on the “high summer” season July and August because the temporal behavior of the SNAO in these months is significantly correlated, unlike June. Nevertheless, as shown by BL87, the spatial pattern of the SNAO in June is quite similar. Like the winter NAO, the existence of the SNAO has important implications for climate extremes such as heavy rainfall and flooding events (e.g., northern European summer 2007). There are, additionally, implications for heat stress caused by high temperatures and for drought in the opposite phase of the SNAO.

We use observational climate datasets and reanalysis data to quantify the effect of the high summer SNAO on surface and tropospheric circulation, surface temperature, cloudiness, rainfall and the position of the Atlantic storm track. In addition, possible SST influences and the temporal variability in the instrumental era (1850 onwards) are examined. This is extended by use of a tree-ring data reconstruction, which permits the SNAO record to be inferred back to 1706. Finally, we show how the SNAO is represented in two coupled climate models, and present projections of SNAO change in enhanced CO₂ simulations that are consistent with anticipated climate change.

2. Eigenvector and cluster definitions of the SNAO

a. Eigenvector definition of the SNAO

We use a definition of the high summer (July–August, henceforth JA) NAO involving an empirical orthogonal function (EOF) covariance analysis of extratropical North Atlantic–European mean sea level pressure anomalies for 1881–2003. Data are taken from a daily MSLP analysis by Ansell et al. (2006); the first eigenvector is defined to be the SNAO (Fig. 1a). We do not use earlier, less accurate data back to 1850 to define the SNAO pattern in case of distortion of the pattern in data sparse high latitudes. We do, however, create time series back to 1850 using this pattern. We tested whether there are differences in the pattern of the SNAO when daily, 10-day mean or July and August mean MSLP data are used. The patterns are almost identical between these time scales over the period 1881–2003. The only appreciable difference lies in the percentage of total variance explained by the SNAO pattern on each time scale. It explains 18.0% of the daily variance, 22.6% of the 10-day mean variance, and 28.3% of the 2-month mean variance over the analysis domain. For the remainder of this paper, we have chosen to use the daily pattern as this allows the day-by-day contribution of the SNAO to a seasonal anomaly to be estimated.

The second daily EOF for high summer explains 14.5% of the variance and is a more zonal pattern with centers over the central North Atlantic and northwest Europe. The third EOF explains 12.1% of the daily variance and has a dipole in the western North Atlantic. The locations of the nodes of the dipole are broadly similar to the positions of maximum negative correlation at 700 hPa between the lower-middle and higher latitudes of the Atlantic region found by Portis et al. (2001) in their “mobile NAO” analysis for July and August. Our analysis using 2-month means is nearest in time scale to their analysis, so Fig. 1b shows the pattern of the JA mean SNAO, again EOF1 as above, while the second July–August mean EOF is similar to the July or August pattern of Portis et al., explaining 19.1% of the JA mean variance. Thus this mode is more prevalent for data averaged over two months. We conclude that the mobile summer NAO found by Portis et al. (2001) is likely to be similar to the second most prominent high summer atmospheric circulation pattern in the extratropical North Atlantic region for data averaged over two months and the third most prominent EOF on daily as well as 10-day time scales (not shown). We note in passing that the actual duration of individual SNAO or mobile summer NAO events is mostly considerably shorter than two months.

b. Cluster analysis definition

A version of k -means cluster analysis of the daily July and August MSLP data using a simulated annealing algorithm (Philipp et al. 2007; Fereday et al. 2008) over 1881–2003 gives similar results. Here we use $k = 10$, for which two clusters appear as almost opposite MSLP anomaly patterns (Fig. 1c). Other reasonable values of k give similar results because the SNAO is so prominent. In absolute MSLP terms, the positive cluster appears as a strong extension of the Azores high over northwest Europe, while the negative pattern emphasizes a relatively deep southward- and eastward-displaced Iceland low. Near symmetry of the two sets of cluster anomalies, unlike the winter NAO (Hurrell et al. 2003; Cassou et al. 2004), indicates that EOF and cluster representations of the SNAO give very similar results. We have therefore used daily EOF1 in this paper in preference to the two SNAO clusters as it is easier to use. Finally we note that these patterns of the high summer SNAO are similar to the first eigenvector of reconstructed 500-hPa height anomalies in a combined eigenvector analysis of June–August 500-hPa height, temperature, and rainfall for the long period 1766–2000 created by Casty et al. (2007). They called this pattern “the blocking mode.”

c. Vertical and temporal structure of the SNAO

Figure 2a shows the regression of MSLP from the NCEP dataset against the July and August mean index of the daily SNAO for the period 1948–2007 to show the Arctic-wide pattern of the SNAO. Figure 2b shows regressions of the daily and 2-month mean high summer North Atlantic Oscillation time series on the daily and 2-month mean NCEP reanalysis 300-hPa height time series for July and August over the period 1948–2003. The surface and 300-hPa patterns are similar, though the Arctic node is weaker at 300 hPa compared to surface. The positive and negative nodes are nearly geographically coincident so the pattern can be described as quasi-equivalent barotropic. However the 10-day (not shown) and 2-month 300-hPa patterns extend a little farther west. All three time scales show a subsidiary weak center over North America; that on the 2-month time scale being relatively the strongest.

Three EOF1 time series are shown in Fig. 3 based on the daily, 10-day, and 2-month mean MSLP EOF1 patterns projected onto the MSLP data for 1850–2007. The time series are very similar, reflecting the similar EOF1 patterns, with a correlation of 0.98 between the 158-yr time series of the high summer average of daily EOF1 and the time series of the 2-month mean EOF1. Multidecadal and interannual variability are very similar. Conclusions in the rest of the paper based on daily EOF1 therefore will apply almost equally well to the 2-month mean EOF1.

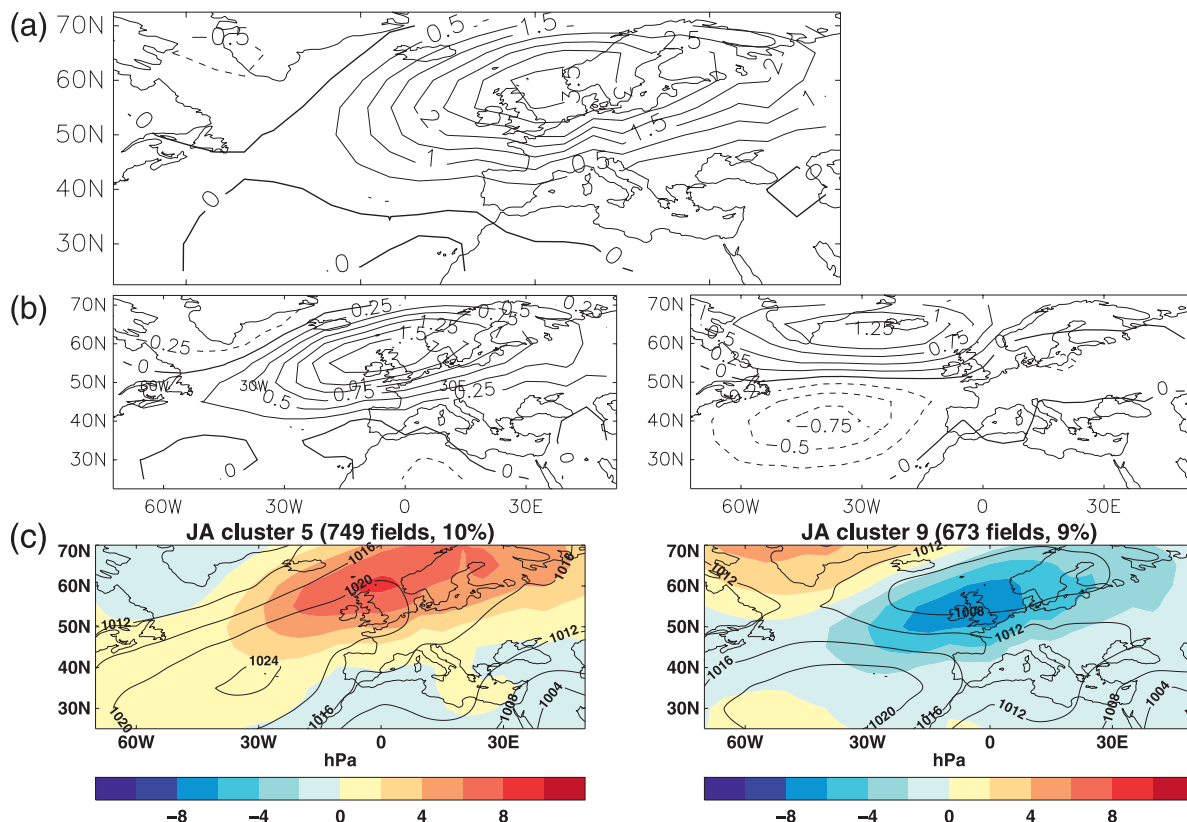


FIG. 1. (a) Pattern of the high summer NAO based on the first covariance eigenvector of anomalies, relative to an 1881–2003 average, of the daily European–North Atlantic mean sea level pressure (EMSLP) dataset for July and August 1881–2003 over the region 25°–70°N, 70°W–50°E. A $5^\circ \times 5^\circ$ grid is used, and the MSLP data are weighted by the square root of each $5^\circ \times 5^\circ$ area when calculating the covariance matrix. Units (hPa) are equal to the local standard deviation of the time series that is explained by the eigenvector. (b) As in (a), but for the (left) first and (right) second EOFs of average July and August pressure at mean sea level data, 1881–2003, over the EMSLP data domain. (c) The positive and negative phases of the high summer NAO shown by a cluster analysis, 1881–2003, of the July–August monthly pressure at mean sea level data of Allan and Ansell (2006). Absolute pressures are contoured black, and anomalies from a seasonally varying climatology are colored. 19% of all days are classified in both clusters together; the clusters are nearly equiprobable.

Table 1 shows the interannual correlations of the daily June, July, and August and July–August SNAO time series. Here we separately calculate the SNAO patterns for June, July, and August in the same way as Fig. 1a. The patterns for July and August are both EOF1 (18.0% and 19.0% of the daily MSLP variance, respectively) and that for June is EOF2 (15.1% of the daily variance). EOF1 for June is quite like the Portis et al. (2001) summer pattern. The three SNAO patterns are almost identical to the July–August SNAO pattern, except that the southern positive node for June extends weakly farther west-southwest. The correlation between the high summer SNAO index and that for June over 1850–2007 is only 0.11; the correlations for July and August are 0.75 and 0.79, respectively. The separately defined July and August indices are significantly intercorrelated at the 5% level, though the value is only 0.20 over 1850–2007 showing the large internal variability in the extratropics on the

monthly time scale. However, the relative intercorrelations of June, July, and August are broadly similar in the two subperiods 1850–1928 and 1929–2007 (see Table 1). Of particular importance is interdecadal behavior in recent decades. Baines and Folland (2007) showed that the high summer SNAO index was related to many time series around the world, partly through the increased index values in the 1960s and 1970s and reduced values since the mid-1980s. Both July and August SNAO indices show this behavior more obviously than the June index values (not shown). Furthermore, recent moderate reductions in the July and August SNAO indices are similar. Overall, the June SNAO index has varied relatively little on these time scales in recent decades.

In conclusion we regard the temporal behavior of the June index to be sufficiently different from those in July and August, and the latter to be sufficiently similar,

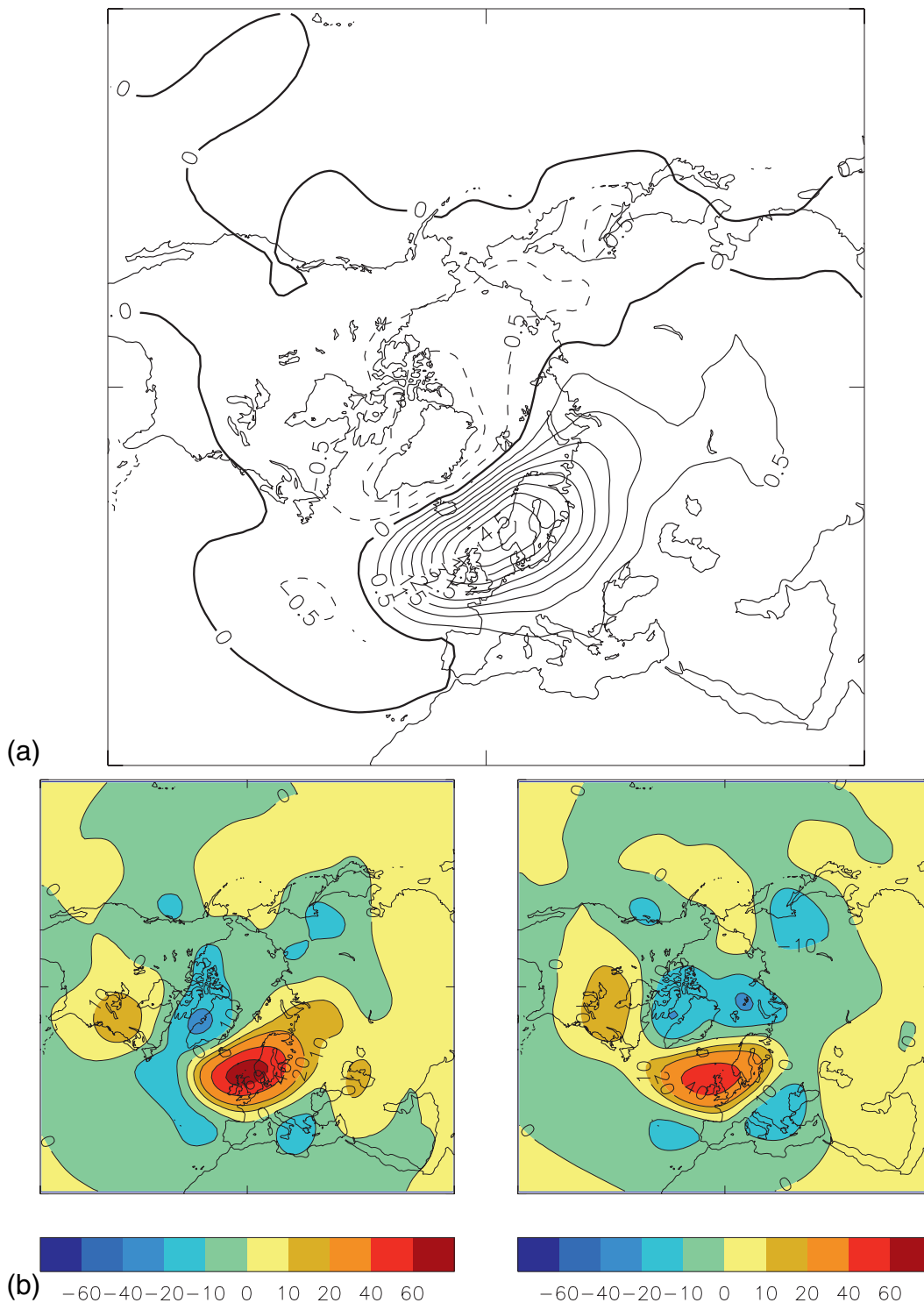


FIG. 2. (a) Regression of pressure at mean sea level at each grid point using the daily NCEP reanalysis dataset against the July and August mean index of the daily high summer NAO, 1948–2007, to show the Arctic-wide pattern of the SNAO. Units are $\text{hPa} (\text{std dev})^{-1}$ of the SNAO time series. The positive center is slightly stronger than for the EMSLP dataset period 1881–2003. (b) Regression of the (left) daily and (right) 2-month mean high summer NAO time series at each grid point on the global daily and 2-month mean NCEP reanalysis 300-hPa-height time series for July and August over the period 1948–2003. Contours are every 20 $\text{m} (\text{std dev})^{-1}$ of the SNAO time series except for the first 10-m contour.

Comparison of daily, 10 day and 2 month EOF1 SNAO series, 1850–2007
Data are standardised over 1881–2003

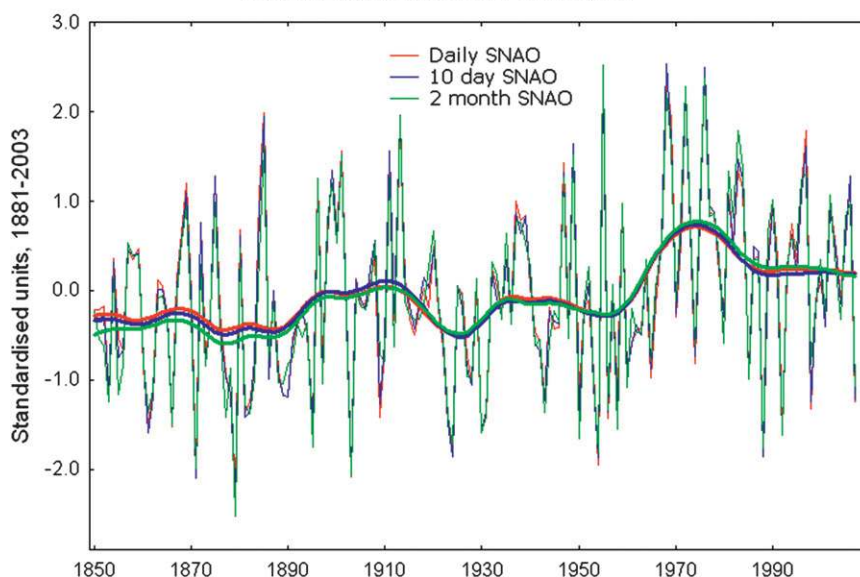


FIG. 3. Time series, 1850–2007, of the standardized July and August average of the daily time series of the daily high SNAO, the July and August average of the 10-day high SNAO and the July and August high SNAO. Low-frequency lines of the same color are low-pass binomially filtered with a half amplitude of 25 yr.

especially on interdecadal time scales, to concentrate on the high summer season.

3. The summer North Atlantic Oscillation, temperature, rainfall, cloudiness, and storm tracks

For the relatively well-observed period 1900–2006, correlations of the SNAO index with worldwide surface temperature (Brohan et al. 2006) are shown in Fig. 4. The left panel is based on periods < 10 yr, while the lower panel illustrates the correlations for periods > 10 yr. A highly statistically significant positive correlation over northwest European land from Ireland to the eastern Baltic is evident for both period ranges, although it is slightly stronger in the shorter periods. Such strong positive correlations are expected as the positive phase of the SNAO corresponds to anticyclonic and thus sunny conditions (see below) over this region, which in summer raises surface temperature through additional sensible heating as discussed further below in this section. Negative correlations are evident over the eastern Mediterranean region in both panels, suggesting increased cloudiness (see below). There is also a significant positive correlation over the width of the Sahel/Sudan region of North Africa for periods < 10 yr, suggesting warmer-than-normal conditions in this region of the West African monsoon tend to accompany the

positive SNAO. This is less clear for periods > 10 yr, although this is more affected by the sparseness of Sahel/Sudan temperature data. Both panels show cold conditions near Greenland, consistent with the cyclonic anomalies indicated in Figs. 1a,c. There is a hint of a positive correlation over northeastern North America in

TABLE 1. Interannual correlations of individual monthly and high summer SNAO time series. Starred values are statistically significant at the 5% level. There is no significant autocorrelation in any of the series.

(a) 1850–2007			
	July	August	SNAO
June	0.11	0.06	0.11
July		0.20*	0.75*
August			0.79*
(b) 1850–1928			
	July	August	SNAO
June	0.21	0.04	0.17
July		0.23*	0.78*
August			0.78*
(c) 1929–2007			
	July	August	SNAO
June	0.01	0.06	0.05
July		0.15	0.72*
August			0.79*

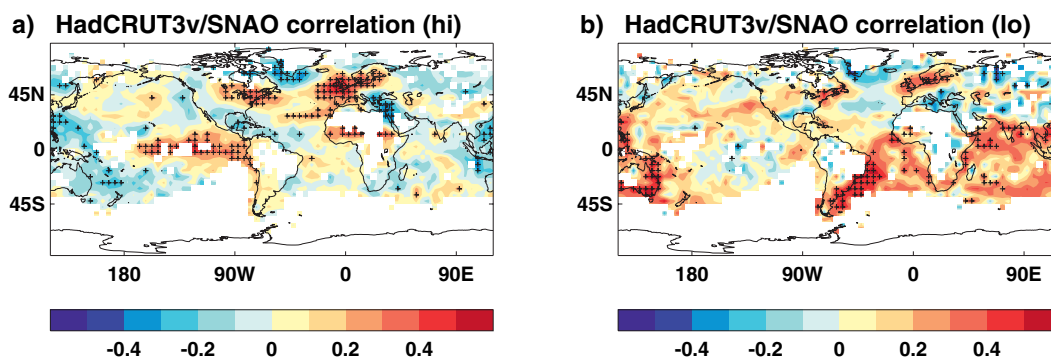


FIG. 4. (a) Simultaneous correlation of worldwide land surface temperature (2 m) air temperature and sea surface temperature, 1900–2007, with the July–August mean of the daily high SNAO using the Hadley Centre Climatic Research Unit version 3 (HadCRUT3v) dataset (Brohan et al. 2006). Temperature and SNAO data are high-pass filtered for periods <10 yr. Crosses represent correlations locally significant at the 5% level. For a correlation to be calculated, $\geq 50\%$ of the possible temperature data had to be present. Significance is assessed using a two-tailed test based on correlating temperature at each grid point with 1000 time series, derived by randomly reordering and then appropriately filtering the original SNAO series. Autocorrelation of the original SNAO series is not significantly different from that of the randomly reordered SNAO series used in significance testing. (b) As in (a) but for periods >10 yr.

both panels; there is no signal evident there in MSLP (Fig. 2a) but there is a positive height anomaly center at 300 hPa that accompanies the positive summer SNAO (Fig. 2b).

There are more striking differences in the correlation patterns over the oceans. For periods <10 yr, there are moderate correlations with an El Niño SST pattern in the tropical East Pacific. This is absent for periods >10 yr; however, the SNAO appears to be related to a quasi-global SST pattern reminiscent of the negative phase of the so-called Atlantic multidecadal oscillation (AMO; e.g., Goldenberg et al. 2001; Knight et al. 2005). The AMO is rather like EOF3 of low-frequency global SST variations in Parker et al. (2007), the similar pattern in Folland et al. (1999), and the interhemispheric pattern in Folland et al. (1986). Sutton and Hodson (2005) and Knight et al. (2006) show in modeling studies, and Baines and Folland (2007) show in their observational study, that summer surface pressure in the northwest European region is likely to be reduced by warming and increased by cooling of SSTs over the North Atlantic as a whole.

An analysis of unfiltered total cloudiness correlated with the SNAO (Fig. 5) is based on a homogenized database derived from the Extended Edited Cloud Reports from Ships and Land Stations over the Globe, 1952–96 (Hahn and Warren 1999) and the Cloud Climatology for Land Stations Worldwide, 1971–96 (Hahn and Warren 2003), and so is restricted to recent decades. This provides more insight into the temperature patterns in Fig. 4. In the positive index phase of the SNAO, northwest Europe experiences significantly reduced cloudiness consistent with positive temperature anomalies, while over the eastern Mediterranean cloudiness

is significantly increased in this phase. South and east of Greenland there is increased cloudiness as expected from the negative sign of the SNAO pattern (Figs. 1a,c). Some of the more subtle features of the SNAO over North America, particularly a weak warming for the positive SNAO phase, are supported by the physical consistency with changes in cloudiness.

Very strong and significant anticorrelations of the SNAO index with JA rainfall (Mitchell and Jones 2005) over northwest Europe are shown in Fig. 6. These exceed -0.64 over parts of the British Isles and widely exceed -0.48 over the area of northwest Europe having strong warm anomalies (Fig. 4) and less clouds (Fig. 5). The relationship with England and Wales rainfall (Wigley et al. 1984) in July and August for 1850–2007 (Fig. 6b) is highly significant (correlation = -0.63 ; note that the rainfall data are reversed). Over the two independent periods of nearly equal length (1850–1928 and 1929–2007) the correlations are also individually significant at -0.56 and -0.66 , respectively, with similar means and standard deviations in each period. Moreover, interdecadal variations of both quantities follow each other very closely with the increase in the SNAO index and decrease of precipitation in the 1960s and early 1970s being particularly prominent, as noted by Baines and Folland (2007) for southeast England rainfall.

Southern European rainfall is significantly positively correlated with the SNAO index, with correlations up to 0.3. The region where rainfall is affected extends farther west than the region with negative temperature correlations. The cloudiness data in Fig. 5 are in agreement with this extra rainfall. Also of interest are negative

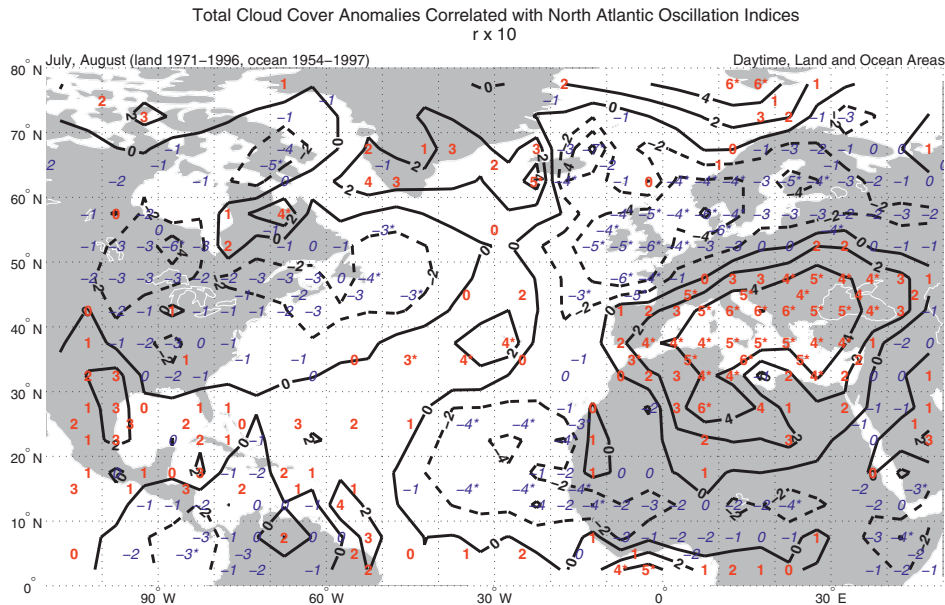


FIG. 5. Correlation of July–August cloudiness with the SNAO. Correlations are multiplied by 10 and cover the period 1971–96 over land and 1954–97 over the oceans. Negative correlation isopleths are dashed and positive are solid. The resolution of the cloudiness data is $5^\circ \times 5^\circ$ over land but only $10^\circ \times 10^\circ$ over the oceans south of 50°N , $10^\circ \text{ lat} \times 20^\circ \text{ lon}$ over the ocean region $50^\circ\text{--}70^\circ\text{N}$ and $10^\circ \times 40^\circ \text{ lon}$ between 70° and 80°N . Starred values have a local significance of 5% or better. Over land this is measured by the average correlation in a given box derived from correlation values at several stations using the Fishers Z statistic.

rainfall correlations over the whole width of the African Sahel, reaching -0.5 in a few places, and the weak positive correlations to its south. This North African precipitation dipole feature is consistent with a southward-displaced and possibly more intense North African intertropical convergence zone (e.g., Rowell et al. 1992) when the SNAO is in its positive index phase. Although the cloudiness data only show weak correlations, they are in the correct sense for lower rainfall and higher temperature (Fig. 4) to be associated with positive SNAO index over the Sahel. Hurrell and Folland (2002) noted a similar relationship with Sahel rainfall. Finally, Figs. 4b and 6 are consistent with the results of Rowell (2003) who analyzed physical reasons for an influence of Mediterranean SSTs on Sahel rainfall, especially on decadal time scales.

We conclude that the North Atlantic region cloudiness correlation pattern is consistent with the SNAO MSLP and surface temperature and rainfall patterns, with a lower cloudiness associated with higher temperatures, more sensible heating, and dry conditions, and a higher cloudiness associated with cooler temperatures, less sensible heating, and wetter conditions, as would be expected in summer. There also appear to be distant relationships between the SNAO and the West African monsoon on a range of time scales.

Variations of the SNAO are associated with changes in the North Atlantic storm track (Fig. 7) such that a positive (negative) SNAO index is associated with its northward (southward) movement over northwest Europe and into the east Atlantic. In the late nineteenth and early twentieth century the SNAO index was generally more negative (Fig. 3) compared to the period after the mid-1960s. The storm track strengthened over Iceland and the Norwegian Sea in the latter period and weakened farther south, particularly over central-western Europe. Thus changes in temperature and rainfall in regions most affected by changes in the SNAO result from a combination of thermodynamic and dynamical effects. Taking England as an example, the positive index phase of the SNAO corresponds to anomalous easterly winds advecting warm air from continental Europe (implied by Fig. 1a) as well as more local solar radiation and surface sensible heating. These effects reinforce the temperature and rainfall response, resulting in the SNAO being a very important control on summer heat, drought, and flooding in northwest Europe. It is less effective over southern Europe as the correlations with surface climate are lower, so that other summer atmospheric patterns are likely to be at least as important (Cassou et al. 2005).

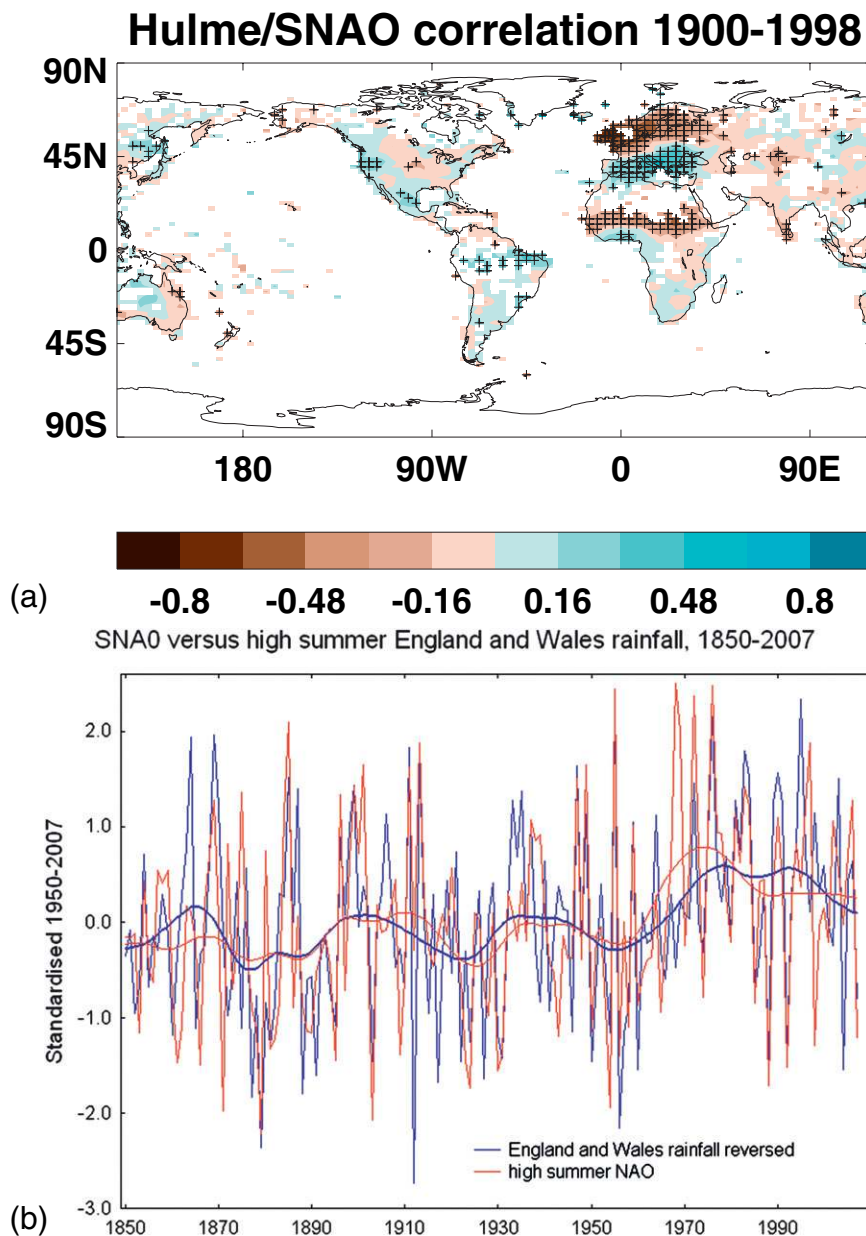


FIG. 6. (a) Simultaneous correlation of worldwide July and August land rainfall over the land with the high SNAO, using the Mitchell and Jones (2005) rainfall data for 1900–98. No filtering has been done. Significance is assessed in a similar way to Fig. 4. (b) The SNAO and July–August England and Wales rainfall, 1850–2007. The rainfall data have been reversed in sign and both series are standardized over 1850–2007. The smooth lines are low-pass filtered for periods >25 yr.

4. Interannual and interdecadal variations of the SNAO in relation to ENSO and the AMO

a. Interannual time scales and ENSO

It was shown in Fig. 4 that local SST is affected by the SNAO, with warm anomalies associated with the southern node of the positive SNAO phase stretching from west of the United Kingdom through the North

Sea to the Baltic, and cold anomalies in the eastern Mediterranean associated with enhanced cloudiness (Fig. 5). The region around southern Greenland is cold in this phase of the SNAO as a result of cyclonic and cloudy conditions there.

In addition to these features, there is a weak (correlation 0.3–0.4) but widespread and locally statistically significant positive correlation with SST in the ENSO

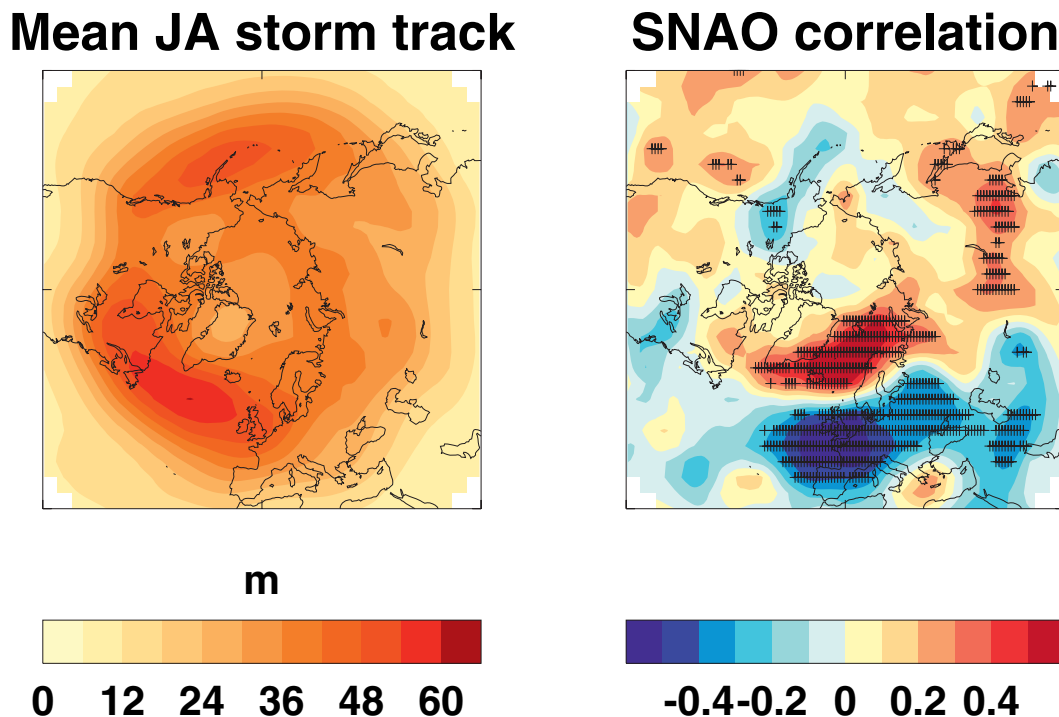


FIG. 7. (left) Mean storm tracks for 1948–2007 in July–August shown by the standard deviation of the 300-hPa geopotential height (m) calculated from daily data and bandpass filtered on time scales of 2–8 days. (right) Simultaneous correlation of the standard deviation of similarly filtered July–August values of 300-hPa height, 1948–2007, with the July–August SNAO index. Crosses represent correlations locally significant at the 5% level using a two-tailed significance test at the 5% level obtained by correlating 1000 randomly reordered versions of the SNAO time series.

region of the tropical Pacific. This suggests, assuming linearity, that a positive SNAO phase is associated with El Niño and a negative SNAO phase with La Niña. The direct correlation of the SNAO and the July–August Niño-3.4 (5°N – 5°S , 170° – 120°W) index [taken from the Rayner et al. (2003) Hadley Centre Sea Ice and Sea Surface Temperature dataset (HadISST) analysis] over the period 1876–2007 is 0.22, which is just significant at the 5% level. Shorter periods give similar correlations, consistent with HadISST being reliable since 1876 for analyzing ENSO SSTs over the tropical east Pacific (Folland et al. 2001) and consistent with the existence of a link throughout the period. To account for the possible time lag between SST changes in the Pacific and effects in the Atlantic extratropics, June and July Niño-3.4 SST was also investigated, but this gave slightly lower correlations with the SNAO indices. At longer lead periods at this time of the year, Niño-3.4 SST anomalies are on average changing rapidly from small values and so will not provide more predictive information.

In Fig. 8, the relationship between the HadISST-derived JA Niño-3.4 index and JA MSLP data from

the Second Hadley Centre Sea Level Pressure dataset (HadSLP2) computed over the period 1876–2006 is investigated. Significant positive regressions (Fig. 8a) exist over much of the Arctic region extending as far south as the north coast of Scotland and east to northern Scandinavia, with significant negative regressions in the North Pacific. The regression coefficient over northern Scotland and northwest Norway is modest ($\sim 0.6 \text{ hPa } ^{\circ}\text{C}^{-1}$). We note, however, that the MSLP data (Allan and Ansell 2006) are distinctly poorer over the higher latitudes of Canada and Greenland before the 1940s, which may reduce the variance there and hence diminish the regression coefficient. Over the northeast Atlantic and Europe, the MSLP data should be reasonably reliable throughout the period.

The composite analyses of Figs. 8b,c show that the regression relationship of Fig. 8a is indeed linear to first approximation, with broadly opposite MSLP anomalies in a given place for El Niño and La Niña conditions. The relationship is such that La Niña (negative Niño-3.4 SSTs) tends to give significantly lower MSLP over European latitudes near 60° – 65°N with anomalous westerly winds to the south. El Niño produces the opposite

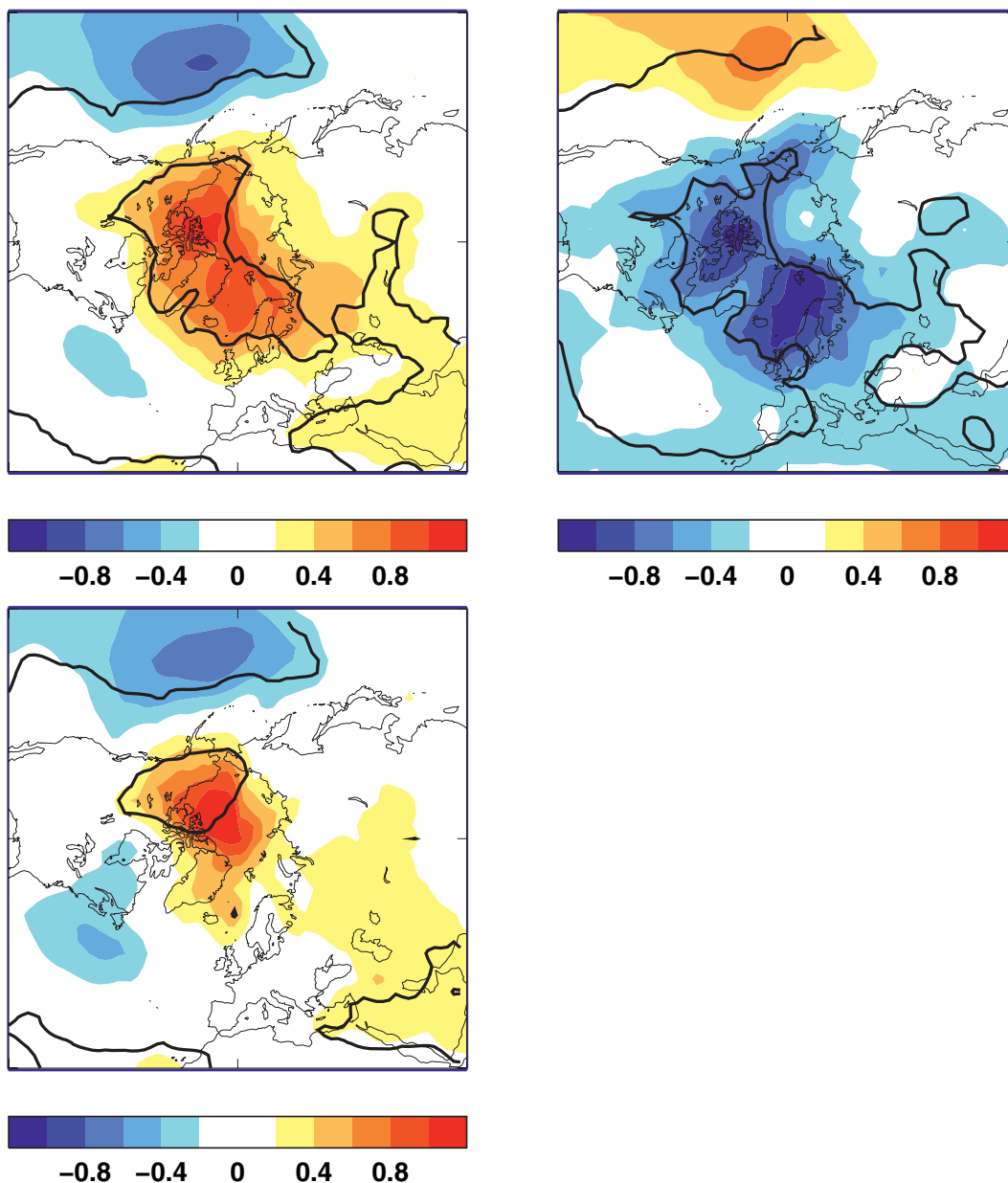


FIG. 8. ENSO relationship with JA MSLP. (top left) Regression of JA Niño-3.4 against JA pressure at mean sea level over 1876–2007 in $\text{hPa } ^\circ\text{C}^{-1}$ (colors). Contours show the edge of regions where regressions are significant at the 95% level of a two-tailed t test. (top right) Composite MSLP anomaly (with respect to the mean of 1901–2000) for the coolest 20% of the Niño-3.4 JA seasons (La Niña case, with Niño-3.4 $< -0.59^\circ\text{C}$). Bold black lines show the edge of regions where the mean La Niña MSLP is statistically different from the remainder of cases at the 95% level. Units are hPa . (bottom) As in (top right), but for the warmest 20% of the Niño-3.4 JA seasons (El Niño case, Niño-3.4 $> 0.44^\circ\text{C}$).

influence but this is weaker and not significant over the SNAO region. In both cases, any effect originating in the tropical Pacific is of the same sign over both the northern and southern nodes of the SNAO; thus, ENSO influences project onto the SNAO only weakly. The main effect is to give a weak tendency to westerly wind or cyclonic anomalies and a negative SNAO phase in La

Niña conditions over northwest Europe. The effect on the SNAO of El Niño conditions is too small to discern in this analysis.

b. Interdecadal time scales and the AMO

On interdecadal time scales, Baines and Folland (2007) suggest a link between the SNAO and the pattern

of the AMO SSTs globally. The AMO is thought to be partly related to natural changes in the thermohaline circulation (Knight et al. 2005, 2006). An important part of this pattern is in the North Atlantic (Delworth and Mann 2000; Enfield et al. 2001; Sutton and Hodson 2005; Knight et al. 2005) such that when the AMO is in its warm North Atlantic phase, the SNAO tends to be in its negative phase. The AMO SST pattern can vary naturally (Trenberth and Shea 2006) or in recent times may have been influenced by anthropogenic aerosols (Rotstayn and Lohman 2002; Mann and Emanuel 2006). Sutton and Hodson (2005) showed in a model analysis using the Third Hadley Centre Atmosphere Model (HadAM3; Pope et al. 2000) that pressure in the north-west European area tends to be lower in the positive phase of the AMO, corresponding therefore to a tendency to a negative SNAO. Knight et al. (2006) showed similar results in summer from a 500-yr control run of the third climate configuration of the Hadley Centre Coupled Model (HadCM3), which simulates the AMO as part of its intrinsic variability. They also show that the simulated central England temperature (CET; Manley 1974; Parker et al. 1992; Parker and Horton 2005) is significantly modulated on decadal time scales. The correlation of modeled June–August CET is highly significant at 0.50 with the modeled AMO. A comparison of observed AMO and SNAO time series is shown in Fig. 9, where the AMO is reversed in sign and both time series have been low-pass filtered. The AMO is taken from a new analysis by Parker et al. (2007); this shows slightly less recent increase than the AMO pattern of Baines and Folland, though it still has an AMO pattern with most weighting in the extratropical North Atlantic. The SNAO and the AMO follow each other fairly closely, though there appears to be an overall trend in the SNAO series to more positive values compared to the AMO series. This relative increasing trend in the SNAO reduces the magnitude of the negative correlation from -0.60 (1850–2007) if the series are detrended to -0.44 if not detrended. The strong filtering does not allow statistical significance to be estimated. The relative SNAO increasing trend component is commented upon further in sections 6 and 7.

Second, Fig. 9 also shows an analysis of the SNAO from an ensemble of 6 HadAM3 experiments from 1871–2002 (see more discussion of modeling the SNAO in section 7). In this ensemble, the model was forced with observed SSTs (from HadISST) as well as with all of the major anthropogenic forcings (Johns et al. 2003). The simulated SNAO variations are rather different from those observed: the strong rise in the observed SNAO index in the 1960s and 1970s is not seen, though the model indicates a delayed but smaller rise in the

AMO EOF index filtered with a half amplitude of 25 years versus similarly filtered observed SNAO, and modelled SNAO

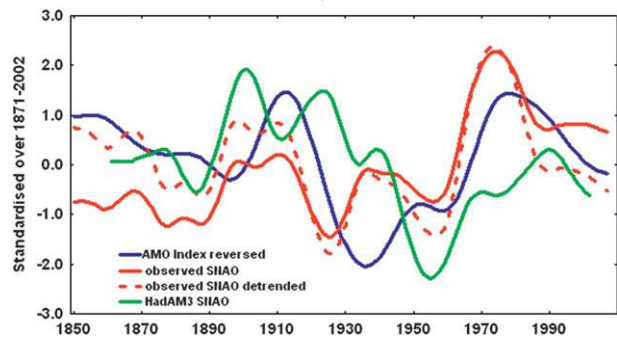


FIG. 9. The AMO SST index reversed (blue) (after Parker et al. 2007) and the observed high SNAO including a detrended version. The modeled SNAO based on the mean of an ensemble of six runs is shown in green. All data are low-pass filtered with a half amplitude of about 25 yr to bring out the relationships of the SNAO with the AMO, and standardized over the period of the model data, 1871–2002. The AMO is thus filtered more strongly than in Parker et al. (2007).

1980s, and the overall correlation with the AMO is only -0.19 . However, the model does capture the observed tendency to a higher SNAO index values when the AMO is in its negative phase.

5. Reconstructing the summer North Atlantic Oscillation back to 1706

a. Reconstructing the SNAO

From instrumental data we can reconstruct the past 150 yr of SNAO behavior. However, it is of considerable interest to determine if the observed multidecadal variability existed in even earlier times. In particular, have the sustained high SNAO index values of the past several decades occurred before? Using tree-ring records, we have extended the SNAO index a further 150 yr into the past.

Trees, especially conifers, growing close to their limits of distribution in the region of the southern node of the SNAO are sensitive to climate during the growing season, that is, summer, (e.g., Briffa et al. 2004). There is a wide range of tree-growth responses to climate in north-western Europe, depending on the growth environment of the trees (altitude, soils, slope etc). In general, because of the proximity of the North Atlantic Ocean, the main growth-limiting factor is high summer temperatures, especially at higher latitudes and altitudes: precipitation is generally plentiful during the growing season, while summers are relatively mild and of short duration. However, it is possible that trees growing in dry, more continental environments may experience drought during exceptionally warm or dry years, and

large amounts of snowfall during winter can affect the following year's growth (e.g., Vaganov et al. 1999). Tree-ring data from the region (especially from Scandinavia) have been used mainly to reconstruct temperatures, but also precipitation, for the last hundreds to thousands of years (e.g., Briffa et al. 2004; Helama and Lindholm 2003; Gouirand et al. 2007). The potential for using tree-ring data to reconstruct large-scale atmospheric features has previously been shown, for example, for the winter mode of the NAO (Cook et al. 1998, 2002). Since the SNAO is associated with marked interannual climate variations in this region, a link between SNAO variability and tree-growth patterns is expected.

We analyzed over 100 tree-ring series (tree-ring widths as well as maximum latewood density) from the region to ascertain their association with the observed SNAO. We used standardized tree-ring data, where negative exponentials or lines of zero or negative slope are used on individual tree-ring series to remove age effects and to preserve the low-frequency signal (Fritts 1976). Highly significant correlations between tree growth and SNAO were found in northern Great Britain and central and northern Norway, with positive correlations in Great Britain and inland Norway and negative correlations on the Norwegian west coast, as would be expected from the correlation patterns shown in Figs. 4a and 6a. Furthermore, the strongest correlations (>0.4) were found over Great Britain. Together, approximately 20 chronologies indicated strong associations with the SNAO, although the lengths of the individual chronologies ranged from 130 to more than 1000 yr. Since our aim was to reconstruct the SNAO for the last three centuries, those seven chronologies reaching as far back or further than 1700 were selected for further analysis (Table 2). Principal component analysis was performed over the 1706–1976 period and used to define the variance common to all chronologies. To reconstruct the SNAO index, a linear regression model, with the observed SNAO as the predictand and significant tree-ring principal components as predictors, was used. The model was initially calibrated using half of the available instrumental data, withholding the remaining data for verification. Consequently, 1850–1912 was first used for calibration and 1913–76 for verification. The procedure was then reversed. The final model, derived from regression over the full period 1850–1976, was used to reconstruct SNAO index back to 1706 (Table 3).

The reconstructed SNAO index compares well with the observed (Fig. 10), although it fails to capture the magnitude of the observed high-frequency variability. There is a slightly stronger association between the reconstructed and observed SNAO indices on interannual ($r = 0.61$) than on decadal to interdecadal ($r = 0.51$)

time scales, but in general the SNAO evolution since 1850 is well captured. A more detailed analysis (not shown) suggests that the reconstruction is actually poorest for periods near 10 yr, and is best on multidecadal periods >25 yr. The full reconstruction (Fig. 10b) shows clear multidecadal variability over 1706–1976, and a tendency toward more positive values of the SNAO in the latter part of the record.

b. Comparison of the reconstructed summer North Atlantic Oscillation, central England temperature, and England and Wales precipitation

We compare the reconstruction of the SNAO index to that of July and August mean CET (Manley 1974; Parker et al. 1992; Parker and Horton 2005). CET is the longest monthly instrumental surface temperature series in the world and well homogenized. It therefore provides a unique opportunity to compare the SNAO with temperature over three centuries, with almost 150 yr of data independent of the calibration and verification period of the proxy SNAO. Figure 11 shows, as expected from the previous discussion, a strong correlation of the SNAO with surface temperature in central England over 1850–2006. In this diagram both series are individually standardized to account for the fact that the standard deviation of the reconstructed SNAO is too small. The region represented by CET does not overlap with that of the tree-ring reconstructions in the previous section but lies centrally within the southern part of the SNAO dipole. So it is reasonable to ask whether a strong relationship is seen between CET and the reconstructed SNAO data before 1850.

Over the period 1706–1976 as a whole, the correlation between July and August CET and the SNAO is 0.55, significant well beyond the 0.1% level. Over the combined calibration and verification period 1850–1976 the value is higher (0.66) as expected. However, over the totally independent period 1706–1849 the relationship remains generally strong ($r = 0.47$) and significant at the 0.1% level. There is some relative loss of variance in the eighteenth century compared to the nineteenth century (Fig. 11) but with little relative loss of correlation ($r = 0.47$ over the eighteenth century). This is despite a period, 1790–1810, where the relationship appears to fail, although there is no obvious extra loss in proxy data reconstruction variability. Similar (but less strong) relationships are seen between the SNAO index and Stockholm temperatures back to 1756 (not shown), with correlations for the 1756–1976 period (0.39), similar to the 1756–1849 period (0.36) and the 1850–1976 period (0.47; all significant beyond the 0.1% level). As with CET, there is also a loss of coherency between these two records centered on 1800, when the reconstructed

TABLE 2. Tree-ring chronologies selected for reconstructing SNAO. The first two columns give the name and country of the site where tree-rings were sampled; the latitude and longitude of the chronologies are given in columns three and four; the fifth column indicates the tree-ring data type used: tree-ring widths (TRW) or maximum latewood density (MXD); the time spans of the chronologies are shown in column six. Data denoted ^a and ^c were obtained from the International Tree-Ring Data Bank, International Geosphere-Biosphere Programme (IGBP) Past Global Changes (PAGES)/World Data Center for Paleoclimatology, National Oceanic and Atmospheric Administration/National Climatic Data Center (NOAA/NCDC) Paleoclimatology Program, Boulder, Colorado.

Name	Country	Lat (°N)	Lon (°E)	Data	Time span (year A.D.)
Forfjorddalen ^a	Norway	68°48'	15°44'	TRW	878–1994
Femundsmarka ^b	Norway	62°00'	12°11'	TRW	1001–2000
Lofoten ^c	Norway	68°29'	16°02'	MXD	1485–1978
Coulin ^c	United Kingdom	57°32'	5°21'	TRW	1671–1978
Coulin ^c	United Kingdom	57°32'	5°21'	MXD	1671–1978
Narvik ^c	Norway	68°29'	17°44'	TRW	1702–1978
Inverey ^c	United Kingdom	53°00'	3°35'	MXD	1706–1976

^a Data from Andreas Kirchhefer.

^b Data from Maarit Kalela-Brundin.

^c Data from Fritz Schweingruber.

SNAO index is in a strongly negative phase. Greatbatch and Rong (2006) noticed a period of loss of correlation between their quite similar version of a July–August SNAO and CET around 1915–25. This is evident in Fig. 11. They attributed this loss of correlation to the dominant influence on high summer CET in this period of a different atmospheric circulation pattern. This gave anomalous anticyclonic or cyclonic conditions over northwest Europe which lacked the extended east–west structure of the southern anticyclonic node of the SNAO; the latter tends to enhance the effects of local differences of cloudiness on CET by advective effects as noted above. Supporting this, the two clusters corresponding to opposite phases of the SNAO (Fig. 1c) are also both slightly less common in the 1915–25 period. Some of the other clusters therefore become more common to compensate, but no single pattern dominates.

A striking feature of Fig. 11 is an overall rise in the SNAO index on multidecadal time scales to a maximum in the 1970s, the end of the data. Given that this higher level has been almost sustained, there appears to be no period back to 1706 when for decades the SNAO was as high. Before 1850 there is a century time-scale fluctuation but no sustained SNAO values higher than in the nineteenth century. CET tends to follow the SNAO

index well on the low-frequency time scale since the late nineteenth century as expected, but before that CET tends to be relatively higher, particularly in the eighteenth century. It is likely that there is a warm bias in eighteenth- and early nineteenth-century high summer instrumental and inferred instrumental data because of poor thermometer exposures (P. Jones 2008, personal communication); some of the early eighteenth-century CET data are also not strictly instrumental (Manley 1974). Although insufficiently reliable on its own to quantify this bias, Fig. 11 suggests the bias might be of the order of one standardized unit or about 1°C in eighteenth-century high summer months relative to the same months in the twentieth century. Thus summer CET may still contain inhomogeneities which would tend to cause an underestimate of the warming of U.K. summer climate over the last 300 yr.

England and Wales precipitation (EWP) is less reliable in earlier decades than CET and rainfall is less well spatially correlated than temperature. EWP also only starts in 1766. So a generally poorer relationship with the SNAO would be expected. Over the calibration and verification period of the SNAO index, the correlation of EWP with the SNAO index is -0.56 and highly significant. Over the independent period 1766–1849 the correlation is still negative but only -0.15 and not

TABLE 3. Calibration and verification statistics against the observed SNAO: r = correlation coefficient, r^2 = explained variance, RE = reduction of error, CE = coefficient of efficiency, and DW = Durbin–Watson statistics.

	Verification				Calibration			
	r	r^2	RE	CE	R	R^2	DW	
1850–1912	0.62	0.38	0.33	0.30	1913–76	0.65	0.43	1.55
1913–76	0.52	0.27	0.31	0.30	1850–1912	0.56	0.32	2.01
					1850–1976	0.62	0.38	1.75

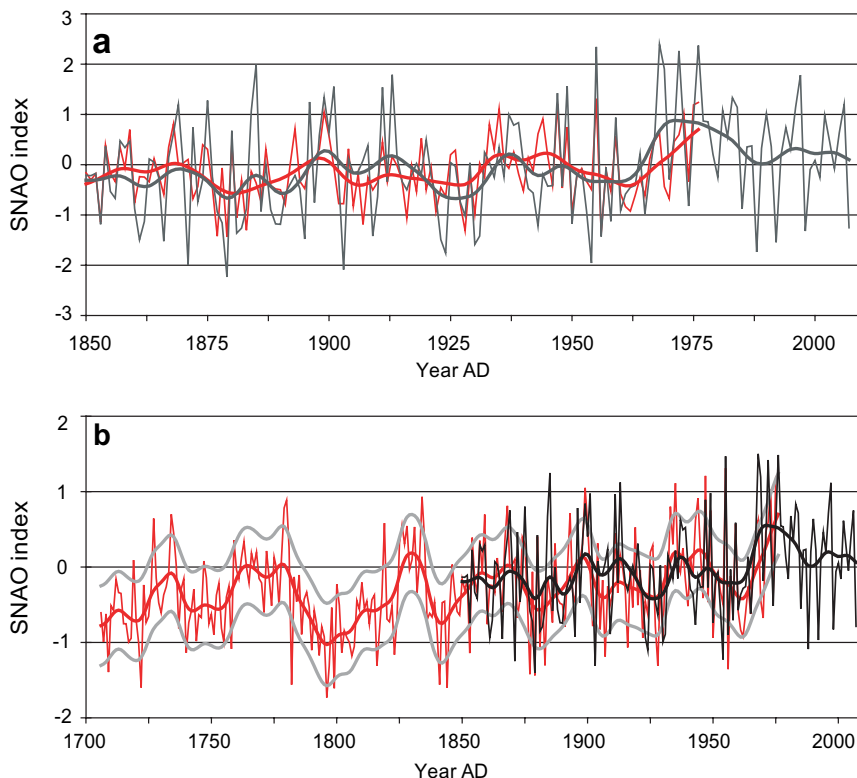


FIG. 10. (a) Reconstructed (red) compared to observed (black) SNAO 1850–1976. Thick lines represent low-frequency variability corresponding to a 10-yr moving average (Gaussian filter with $\sigma = 3$). (b) The SNAO 1706–1976 reconstructed from British and Fennoscandian tree-ring data. Data are shown as interannual (thin red) and smoothed (Gaussian filtered) SNAO, highlighting variability on time scales longer than 10 yr (thick red). The uncertainty in reconstructed SNAO (based on the calibration period statistics) is illustrated by ± 2 standard errors on and decadal time scales (gray, thick line). Also included is the observed SNAO (black lines), where the variance of the time series (interannual = thin line; decadal = thick line) has been adjusted to that of the reconstructed for comparisons sake.

significant, though it is higher in the late eighteenth century (1766–1800) at -0.30 .

6. Simulations and projections of the SNAO

We have used a 500-yr control simulation of the HadCM3 (Gordon et al. 2000) and a 240-yr simulation of the Hadley Centre Global Environmental Model version 1 (HadGEM1; Johns et al. 2006) to examine internal summer North Atlantic–European variability. The first aim is to test whether these models reproduce the observed pattern and amplitude of the SNAO in control mode. Figure 12 shows the patterns of simulated internal variability contained in the first two EOFs of JA MSLP. For HadCM3, the first EOF strongly resembles the observed SNAO (Fig. 2b), despite having centers that are shifted slightly to the southwest and being slightly more zonally elongated. It is clearly distinct from a winter NAO-type pattern, with more northerly

centers, as observed. The peak variability of about 2 hPa is similar to observations, as is the fraction of explained variance (23.2% compared to 28.3% in the observations). Also shown is the pattern of the second EOF (with 14.2% of explained variance), which is also very similar to the second observed EOF (19.1%). The analysis shows that HadCM3 produces a realistic SNAO as the leading mode of summer variability in the North Atlantic–European sector. The first EOF for HadGEM1 (accounting for 26.8% of the interannual variance) does not correspond to the observed SNAO, however, but is very similar to the second EOF in both observations and HadCM3. Rather, it is the second EOF of HadGEM1 (with 18.0% of the variance) that is very similar to the observed SNAO, perhaps even more so than EOF1 in HadCM3. The HadGEM1 model, therefore, produces realistic summer circulation variability, except that it underrepresents the prominence of the SNAO variability.

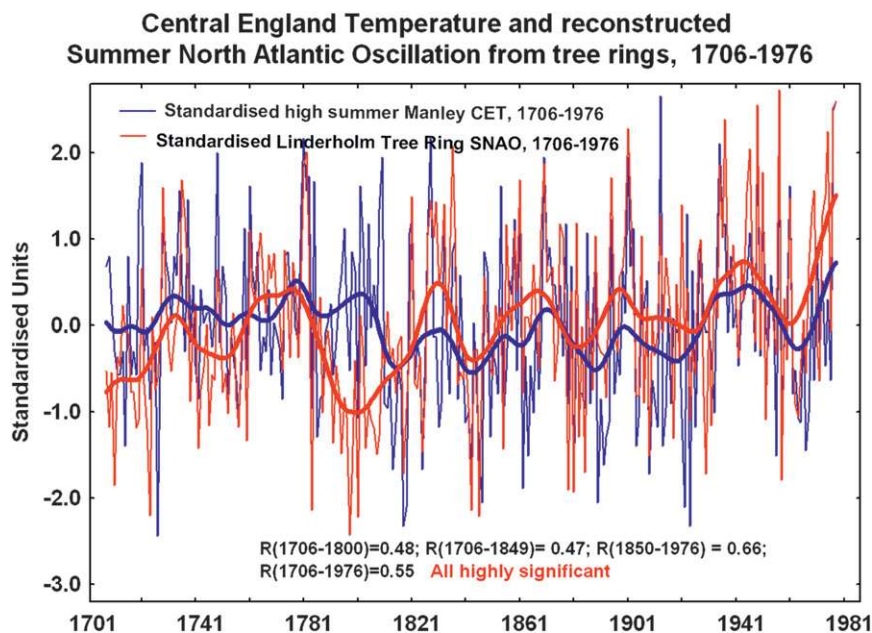


FIG. 11. Comparison of standardized central England temperature and standardized reconstructed SNAO using proxy data as in Fig. 10. Both series are standardized over 1706–1976, the period of the reconstructed data to show the relationships clearly. The calibration and test period for the SNAO was 1850–1976. The smoothed lines are the data low-pass filtered for periods >25 yr.

To investigate possible future changes in the SNAO, we used further HadCM3 and HadGEM1 simulations which were identical to the control experiments except for increasing levels of atmospheric CO_2 . In the HadCM3 transient simulation, CO_2 was increased by $2\% \text{ yr}^{-1}$ for 70 yr, and in the HadGEM1 simulation it was increased by $1\% \text{ yr}^{-1}$ for 140 yr. In both experiments, a level of 4 times the initial, preindustrial CO_2 concentration of 285 ppmv was attained after this time, and was held constant for 100 yr thereafter. We analyze the final 50 yr of the experiments in order to ensure the climate has stabilized and to minimize the influence of the difference in the initial rates of CO_2 increase. These experiments are thought to be a useful, if extreme, analog of future climate change, for which increasing CO_2 is likely to be the dominant driver.

The difference between the mean JA MSLP for the last 50 yr of the steady $4 \times \text{CO}_2$ phase of the transient simulation and the equivalent part of the control simulation is shown in Fig. 13. It is found that there are large-scale reorganizations of atmospheric mass in the altered climate of both models, but particularly in HadCM3. These tend to increase MSLP over the tropical and Southern Hemisphere Pacific Ocean and decrease MSLP over the Northern Hemisphere, especially in the Eurasian sector. As these changes at very large scales are expected to be independent of the synoptic-scale changes

investigated here, we subtract the average MSLP in the region north of 30°N from all grid points globally before continuing the analysis. The resulting patterns of MSLP change are also shown in Fig. 13 and reveal statistically significant changes in circulation. In HadCM3, there are MSLP decreases of over 6 hPa over Greenland and increases of over 3 hPa west of the British Isles. HadGEM1 reveals similar changes, albeit smaller, with a 1-hPa decrease over Greenland and a 2–3-hPa increase over the northern North Sea. These patterns, which are similar to those found in multimodel assessments of future MSLP change (Meehl et al. 2007; Giorgi and Coppola 2007), have strong resemblances to each respective model's SNAO pattern (Fig. 12). The models additionally show other MSLP changes which do not correspond to the SNAO pattern, for example over southern Europe stretching into central Asia. This is to be expected as the SNAO is a regional feature and other responses could occur in other regions. The southern Europe changes are also seen in other models, and appear to be linked to the robust drying signal simulated over this region. Over northern Europe the simulations suggest that the change in circulation will be equivalent to an increasingly positive phase of the SNAO.

To further show this, we also present a time series of the change in the SNAO defined by projecting each model's own SNAO pattern (EOF1 for HadCM3 and

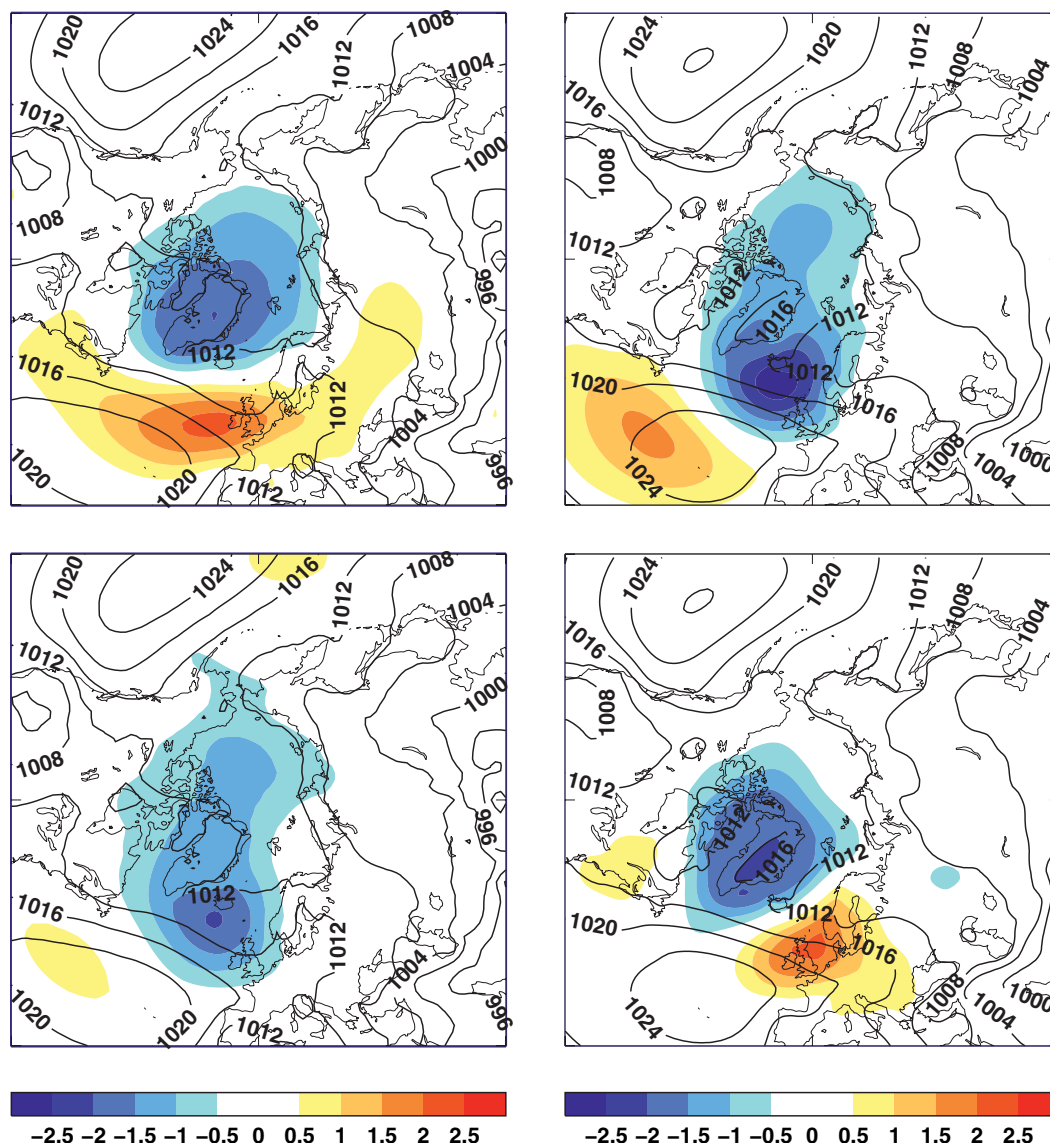
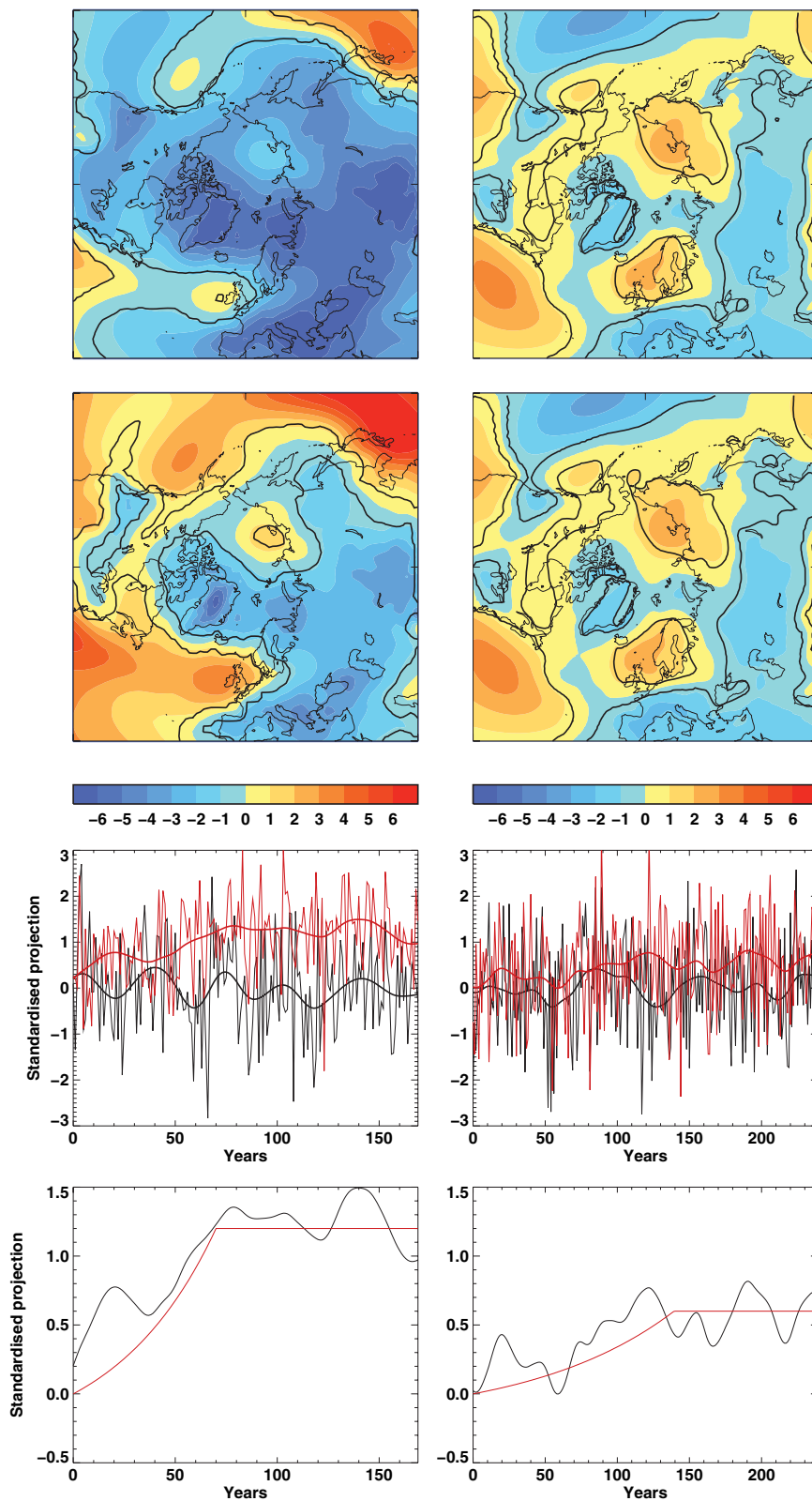


FIG. 12. Leading two EOF patterns of mean JA MSLP in control simulations of (left) HadCM3 and (right) HadGEM1. The HadCM3 EOFs are derived from a 500-yr simulation and the HadGEM1 EOFs are derived from a 240-yr simulation. An area-weighted EOF analysis is performed for the region 25°–70°N, 70°W–50°E, and the resulting standardized principal component is regressed onto the hemispheric MSLP data. Colors indicate the EOF pattern in hPa, while contours show the climatological mean MSLP in hPa. (top) EOF1 accounts for 23.2% of the total variance in HadCM3 and 26.8% in HadGEM1. (bottom) EOF2 accounts for 14.2% of the variance in HadCM3 and 18.0% in HadGEM1. Units are hPa.

EOF2 for HadGEM1) onto the control and transient MSLP data (Fig. 13). We find that for both models the SNAO shifts to more positive values, reaching mean levels in the period 50–100 yr after CO₂ stabilization of 1.22 ± 0.53 (latter value is two standard errors) and 0.53 ± 0.38 standard deviations of the interannual variability in the control simulations for HadCM3 and HadGEM1. SNAO changes are highly significant well beyond the 5% level. These shifts imply that JA seasons

with SNAO index values lower than the control average are rare under conditions of $4 \times \text{CO}_2$ in HadCM3 and still substantially less common (15 in the 50 yr used in the upper panels of Fig. 13) in HadGEM1. Note that the SNAO index increases in both models appear to mirror the time series of the increase and the leveling off of the increase in CO₂ concentration.

It appears that the SNAO may be sensitive to large changes in greenhouse gas forcing, although we do not



know whether the mechanisms are the same as those involved in unforced variability. At the least, the results imply that the climate change response projects onto the SNAO. A typical “business as usual” emissions scenario could, therefore, lead to increased frequency of positive SNAO conditions and so warmer and drier northwest European summers. In HadCM3, there are indeed extreme reductions in JA rainfall across the whole of Europe, peaking at greater than 80% over western France for the 50-yr period used in Fig. 12. Over the British Isles, where the HadCM3 SNAO has most effect, reductions between 20% and 80% are projected. Rowell and Jones (2006) show similar, if smaller, drying signals across most of Europe in a simulation with a higher resolution HadCM3 version for 2071–2100 using the Special Report on Emissions Scenarios (SRES A2, which has projected CO₂ concentrations of about 2.5 times preindustrial levels). Large drying is also seen in HadGEM1, but as with the MSLP response, the magnitude is smaller than HadCM3. Peak reductions in rainfall of 60%–80% are predicted over southern France and northern Spain, with reductions over the British Isles of 20%–60%. Changes over southern and central Europe may also result from shifts in the position and intensity of the subtropical anticyclone, but this is unlikely to influence northern Europe directly. Rather, a contribution from the more positive SNAO is likely. Support for this idea is provided by Rowell and Jones (2006), who were able to separate European climatic changes arising through remotely generated large-scale atmospheric changes from those arising from intrinsic climatic warming by creating an isolated European domain within their model. They found that the most important factor in the simulated precipitation reductions in southern and central Europe is climatic warming and drying of the soils, whereas for northern and western Europe (which corresponds to the southern node of the SNAO), circulation-related factors play the more important role. Our results and those in Rowell and Jones (2006) indicate that climate change is likely to cause a dramatic

increase in droughts and the incidence of heat stress throughout most of Europe for a combination of reasons. Circulation-related changes in climate are over and above the circulation-independent warming anticipated from greenhouse gas increases.

7. Conclusions

The North Atlantic Oscillation (NAO) is the most important single mode for interpreting winter climate variability in the North Atlantic European sector. It is expressed as changes in westerly winds over the North Atlantic region and as a result is the primary determinant of temperatures and storminess in the European winter. Since the winter months are dynamically the most active, most focus has previously been on the winter NAO. Here we have shown that there exists a pattern of variability we call the summer North Atlantic Oscillation (SNAO), which is the summertime parallel to the winter NAO. It is able to explain the principal variations of summer climate over northern Europe, including mean temperatures, precipitation, and cloudiness. While SNAO-like patterns have previously been identified (BL87; Hurrell and van Loon 1997; Hurrell and Folland 2002; Hurrell et al. 2003; Cassou et al. 2005), a definitive analysis is provided here for the first time. Lack of this has led to disagreement in the scientific literature about the pattern of the principal summer mode in the North Atlantic sector. An important part of this confusion arises from the more northerly position and smaller spatial extent of the SNAO compared to its winter counterpart.

The SNAO is defined as the first eigenvector of daily extratropical North Atlantic–European MSLP during high summer (July–August; Figs. 1a and 2a). These two months were chosen for analysis because the July and August time series of the SNAO pattern vary in a broadly similarly way, especially on interdecadal times scales whereas June varies differently. However, the spatial signature of the June SNAO pattern is quite

←

FIG. 13. MSLP changes in response to $4 \times \text{CO}_2$ forcing in (left) HadCM3 and (right) HadGEM1. (top) The raw model differences for the last 50 yr of data starting 50 yr after CO₂ stabilization are shown with respect to the equivalent period in the control simulation. (upper middle) Differences with the mean MSLP difference north of 30°N subtracted everywhere over the globe are shown in an attempt to remove the summer hemispheric mean climate change signal of reduced MSLP. Units are hPa. (lower middle) The SNAO index defined as the projection over the SNAO area (50°–80°N, 60°W–30°E) of the model first (for HadCM3) or second (for HadGEM1) EOF (computed over 25°–70°N, 70°W–50°E) for control (black) and transient (red) simulations. The projections are normalized with respect to the control standard deviation. Low-pass filtered projections are denoted by the thick curves. (bottom) The low-frequency curves are reproduced, along with scaled curves showing the models’ CO₂ increases above the preindustrial level.

similar to the other high summer months. The resulting SNAO is a temporally stable pattern on daily to bi-monthly time scales (Fig. 3a), explaining 18% (daily) to 28% (2-month mean) of the variance of a principal component analysis over the analysis domain. In addition, the SNAO has a quasi-equivalent barotropic structure. The positive phase of the SNAO is associated with warm, dry, and relatively cloud-free conditions over northwest Europe, especially the United Kingdom and much of Scandinavia, and, more weakly, cooler, wetter, and cloudier conditions over southern Europe and the Mediterranean, especially in the east. (Figs. 4, 5, and 6a). Some locally significant correlations are found over northeast North America where higher-than-normal temperatures are related to the positive phase of the SNAO. The evidence for anomalous atmospheric circulation associated with this feature is slight at the surface, but is clearest at 300 hPa and on the 2-month time scale.

Some significant negative correlations with rainfall and cloudiness, and positive correlations with temperature over the African Sahel region suggest distant relationships between the SNAO and the West African monsoon in July and August. These relationships are consistent with links between multidecadal and interannual variations in North Atlantic SSTs (and associated SST variations elsewhere) and climate in various parts of the North Atlantic sector, as previously reported by, for example, Folland et al. (1986), Rowell et al. (1995), Delworth and Mann (2000), Sutton and Hodson (2005), Knight et al. (2006). Indeed, for periods greater than 10 yr, the SNAO seems to be linked significantly to the Atlantic multidecadal oscillation (AMO) in both models (e.g., Knight et al. 2006) and the observations shown in this paper. Here the warm and cold North Atlantic phase of the AMO corresponds to a negative and positive phase SNAO, respectively. This is particularly evident in the last few decades as noted by Baines and Folland (2007).

On interannual time scales, small but significant correlations with a La Niña SST pattern in the eastern Pacific appear in high summer. An analysis of the atmospheric patterns associated with El Niño conditions in high summer shows no significant signal with the SNAO.

The SNAO has been reconstructed back to 1706 using tree-ring data from the United Kingdom and western Scandinavia. The reconstruction explains almost 40% of the variance in the observed SNAO in a testing period. Its reconstruction phase, allowing for some loss of interannual amplitude, agrees well with long meteorological records from the United Kingdom and Scandinavia. This can be seen as a measure of the temporal stability of the reconstruction. Taken with the instrumental data, the high positive index values of the SNAO

attained in the period around 1970–95 has no counterpart in the past three centuries. A trend to a more positive SNAO phase is also emerging relative to the variations in the AMO.

Simulations of possible future changes in the SNAO using the HadCM3 and HadGEM1 models, in which atmospheric CO₂ was increased from preindustrial levels until stabilization at 4 times preindustrial concentrations, suggest that the associated change in circulation will indeed be equivalent to an increasingly positive SNAO phase. This result agrees qualitatively with the pattern of change predicted by the Third Coupled Model Intercomparison Project (CMIP3) multimodel ensemble under doubled CO₂ conditions. These results indicate an increased longer-term risk of drought in northwest Europe. Looking a couple of decades ahead to around 2030, the AMO, or at least the component related to variations in the Atlantic meridional overturning circulation, may have turned down both naturally (Knight et al. 2005) and because of enhanced greenhouse gases (Meehl et al. 2007). This could cause a change to a more positive SNAO, with enhanced droughts and heat waves over northwest Europe setting in around that time.

Acknowledgments. The Met Office authors were supported by the Joint Defra and MoD Programme, (Defra) GA01101 (MoD) CBC/2B/0417_Annex C5. Hans Linderholm was supported by the Swedish Research Council (VR). The paper contributes to the CLIVAR Climate of the Twentieth Century International Project and the European Union EMULATE project. The authors thank Ryan Eastman for supplying Fig. 5 and Adam Scaife and Dave Rowell for useful discussions. Two anonymous reviewers improved the paper.

REFERENCES

- Allan, R. J., and T. J. Ansell, 2006: A new globally complete monthly historical gridded mean sea level pressure data set (HadSLP2): 1850–2003. *J. Climate*, **19**, 5816–5842.
- Ansell, T. J., and Coauthors, 2006: Daily mean sea level pressure reconstructions for the European–North Atlantic region for the period 1850–2003. *J. Climate*, **19**, 2717–2742.
- Baines, P. G., and C. K. Folland, 2007: Evidence for a rapid global climate shift across the late 1960s. *J. Climate*, **20**, 2721–2744.
- Barnston, A. G., and R. E. Livezey, 1987: Classification, seasonality and persistence of low-frequency atmospheric circulation patterns. *Mon. Wea. Rev.*, **115**, 1083–1126.
- Briffa, K. R., T. J. Osborn, and F. H. Schweingruber, 2004: Large-scale inferences from tree rings: A review. *Global Planet. Change*, **40**, 11–26.
- Brohan, P., J. J. Kennedy, I. Harris, S. F. B. Tett, and P. D. Jones, 2006: Uncertainty estimates in regional and global observed

- temperature changes: A new dataset from 1850. *J. Geophys. Res.*, **111**, D12106, doi:10.1029/2005JD006548.
- Cassou, C., L. Terray, J. W. Hurrell, and C. Deser, 2004: North Atlantic winter climate regimes: Spatial asymmetry, stationarity with time, and oceanic forcing. *J. Climate*, **17**, 1055–1068.
- , —, and A. S. Phillips, 2005: Tropical Atlantic influence on European heat waves. *J. Climate*, **18**, 2805–2811.
- Casty, C., C. C. Raible, T. F. Stocker, H. Wanner, and J. Luterbacher, 2007: A European pattern climatology 1766–2000. *Climate Dyn.*, **29**, 791–805, doi:10.1007/s00382-007-0257-6.
- Cook, E. R., R. D. D'Arrigo, and K. R. Briffa, 1998: A reconstruction of the North Atlantic Oscillation using tree-ring chronologies from North America and Europe. *Holocene*, **8**, 9–17.
- , —, and M. E. Mann, 2002: A well-verified, multiproxy reconstruction of the winter North Atlantic Oscillation index since AD 1400. *J. Climate*, **15**, 1754–1764.
- Delworth, T. L., and M. E. Mann, 2000: Observed and simulated multidecadal variability in the Northern Hemisphere. *Climate Dyn.*, **16**, 661–676.
- Enfield, D. B., A. M. Mestas-Núñez, and P. J. Trimble, 2001: The Atlantic multidecadal oscillation and its relation to rainfall and river flows in the continental U.S. *Geophys. Res. Lett.*, **28**, 2077–2080.
- Feldstein, S. B., 2007: The dynamics of the North Atlantic Oscillation during the summer season. *Quart. J. Roy. Meteor. Soc.*, **133**, 1509–1518.
- Fereday, D. R., J. R. Knight, A. A. Scaife, C. K. Folland, and A. Philipp, 2008: Cluster analysis of North Atlantic–European circulation types and links with tropical Pacific Sea surface temperatures. *J. Climate*, **21**, 3687–3703.
- Folland, C. K., D. E. Parker, and T. N. Palmer, 1986: Sahel rainfall and worldwide sea temperatures 1901–85. *Nature*, **320**, 602–607.
- , —, A. Colman, and R. Washington, 1999: Large scale modes of ocean surface temperature since the late nineteenth century. *Beyond El Niño: Decadal and Interdecadal Climate Variability*, A. Navarra, Ed., Springer-Verlag, 73–102.
- , and Coauthors, 2001: Observed climate variability and change. *Climate Change 2001: The Scientific Basis*, J. T. Houghton et al., Eds., Cambridge University Press, 99–181.
- Fritts, H. C., 1976: *Tree Rings and Climate*. Academic Press, 567 pp.
- Giorgi, F., and E. Coppola, 2007: European climate-change oscillation (ECO): 2007. *Geophys. Res. Lett.*, **34**, L21703, doi:10.1029/2007GL031223.
- Goldenberg, S. B., C. W. Landsea, A. M. Mestas-Núñez, and W. M. Gray, 2001: The recent increase in Atlantic hurricane activity: Causes and implications. *Science*, **293**, 474–479.
- Gordon, C., C. Cooper, C. A. Senior, H. Banks, J. M. Gregory, T. C. Johns, J. F. B. Mitchell, and R. A. Wood, 2000: The simulation of SST, sea ice extents and ocean heat transports in a version of the Hadley Centre coupled model without flux adjustments. *Climate Dyn.*, **16**, 147–168.
- Gouirand, I., H. W. Linderholm, A. Moberg, and B. Wohlfarth, 2007: On the spatiotemporal characteristics of Fennoscandian tree-ring based summer temperature reconstructions. *Theor. Appl. Climatol.*, **91**, 1–25, doi:10.1007/s00704-007-0311-7.
- Greatbatch, R. J., and P. P. Rong, 2006: Discrepancies between different Northern Hemisphere summer atmospheric circulation data products. *J. Climate*, **19**, 1261–1273.
- Hahn, C. J., and S. G. Warren, 1999: Extended edited cloud reports from ships and land stations over the globe, 1952–1996. Numerical Data Package NDP-026C, Carbon Dioxide Information Analysis Center, Department of Energy, Oak Ridge, TN, 79 pp.
- , and —, 2003: Cloud climatology for land stations worldwide, 1971–1996. Numerical Data Package NDP-026D, Carbon Dioxide Information Analysis Center, Department of Energy, Oak Ridge, TN, 35 pp.
- Helama, S., and M. Lindholm, 2003: Droughts and rainfall in south-eastern Finland since AD 874, inferred from Scots pine ring-widths. *Boreal Environ. Res.*, **8**, 171–183.
- Horel, J. D., 1981: A rotated principal component analysis of the interannual variability of the Northern Hemisphere 500 mb height field. *Mon. Wea. Rev.*, **109**, 2080–2092.
- Hurrell, J. W., and H. van Loon, 1997: Decadal variations in climate associated with the North Atlantic Oscillation. *Climatic Change*, **36**, 301–326.
- , and C. K. Folland, 2002: A change in the summer circulation over the North Atlantic. *CLIVAR Exchanges*, No. 25, International CLIVAR Project Office, Southampton, United Kingdom, 52–54.
- , Y. Kushnir, G. Ottersen, and M. Visbeck, 2003: An overview of the North Atlantic Oscillation. *The North Atlantic Oscillation: Climatic Significance and Environmental Impact*, *Geophys. Monogr.*, Vol. 134, Amer. Geophys. Union, 1–35.
- Johns, T. C., and Coauthors, 2003: Anthropogenic climate change for 1860 to 2100 simulated with the HadCM3 model under updated emissions scenarios. *Climate Dyn.*, **20**, 583–612.
- , and Coauthors, 2006: The new Hadley Centre climate model (HadGEM1): Evaluation of coupled simulations. *J. Climate*, **19**, 1327–1353.
- Kalnay, E., and Coauthors, 1996: The NCEP/NCAR 40-Year Reanalysis Project. *Bull. Amer. Meteor. Soc.*, **77**, 437–471.
- Knight, J. R., R. J. Allan, C. K. Folland, M. Vellinga, and M. E. Mann, 2005: A signature of persistent natural thermohaline circulation cycles in observed climate. *Geophys. Res. Lett.*, **32**, L20708, doi:10.1029/2005GL024233.
- , C. K. Folland, and A. A. Scaife, 2006: Climatic impacts of the Atlantic multidecadal oscillation. *Geophys. Res. Lett.*, **33**, L17706, doi:10.1029/2006GL026242.
- Manley, G., 1974: Central England temperatures: Monthly means 1659 to 1973. *Quart. J. Roy. Meteor. Soc.*, **100**, 389–405.
- Mann, M. E., and K. A. Emanuel, 2006: Atlantic hurricane trends linked to climate change. *Eos, Trans. Amer. Geophys. Union*, **87**, 233–244.
- Meehl, G. A., and Coauthors, 2007: Global climate projections. *Climate Change 2007: The Physical Science Basis*, S. Solomon et al., Eds., Cambridge University Press, 747–845.
- Mitchell, T. D., and P. D. Jones, 2005: An improved method of constructing a database of monthly climate observations and associated high-resolution grids. *Int. J. Climatol.*, **25**, 693–712.
- Ogi, M., K. Yamazaki, and Y. Tachibana, 2004: The summertime annular mode in the Northern Hemisphere and its linkage to the winter mode. *J. Geophys. Res.*, **109**, D20114, doi:10.1029/2004JD004514.
- , —, and —, 2005: The summer northern annular mode and abnormal summer weather in 2003. *Geophys. Res. Lett.*, **32**, L04706, doi:10.1029/2004GL021528.
- Parker, D. E., and E. B. Horton, 2005: Uncertainties in the central England temperature series 1878–2003 and some improvements to the maximum and minimum series. *Int. J. Climatol.*, **25**, 1173–1188.
- , T. Legg, and C. K. Folland, 1992: A new daily central England temperature series, 1772–1991. *Int. J. Climatol.*, **12**, 317–342.

- , C. Folland, A. Scaife, J. Knight, A. Colman, P. Baines, and B. Dong, 2007: Decadal to multidecadal variability and the climate change background. *J. Geophys. Res.*, **112**, D18115, doi:10.1029/2007JD008411.
- Philipp, A., P. M. Della-Marta, J. Jacobeit, D. R. Fereday, P. D. Jones, A. Moberg, and H. Wanner, 2007: Long-term variability of daily North Atlantic–European pressure patterns since 1850 classified by simulated annealing clustering. *J. Climate*, **20**, 4065–4095.
- Pope, V. D., M. L. Gallani, P. R. Rowntree, and R. A. Stratton, 2000: The impact of new physical parametrizations in the Hadley Centre climate model: HadAM3. *Climate Dyn.*, **16**, 123–146.
- Portis, D. H., J. E. Walsh, M. El Hamly, and P. J. Lamb, 2001: Seasonality of the North Atlantic Oscillation. *J. Climate*, **14**, 2069–2078.
- Rayner, N. A., D. E. Parker, E. B. Horton, C. K. Folland, L. V. Alexander, D. P. Rowell, E. C. Kent, and A. Kaplan, 2003: Global analyses of sea surface temperature, sea ice, and night marine air temperature since the late nineteenth century. *J. Geophys. Res.*, **108**, 4407, doi:10.1029/2002JD002670.
- Rotstayn, L., and U. Lohman, 2002: Tropical rainfall trends and the indirect aerosol effect. *J. Climate*, **15**, 2103–2116.
- Rowell, D. P., 2003: The impact of Mediterranean SSTs on the Sahelian rainfall season. *J. Climate*, **16**, 849–862.
- , and R. G. Jones, 2006: Causes and uncertainty of future summer drying over Europe. *Climate Dyn.*, **27**, 281–299, doi:10.1007/s00382-006-0125-9.
- , C. K. Folland, K. Maskell, and J. A. Owen, 1992: Modelling the influence of global sea surface temperature on the variability and predictability of seasonal Sahel rainfall. *Geophys. Res. Lett.*, **19**, 905–908.
- , —, —, and M. N. Ward, 1995: Variability of summer rainfall over tropical North Africa (1906–92): Observations and modelling. *Quart. J. Roy. Meteor. Soc.*, **121**, 669–704.
- Sutton, R. T., and D. L. R. Hodson, 2005: Atlantic Ocean forcing of the North American and European summer climate. *Science*, **309**, 115–118.
- Thompson, D. W. J., and J. M. Wallace, 1998: The Arctic Oscillation signature in the wintertime geopotential height and temperature fields. *Geophys. Res. Lett.*, **25**, 1297–1300.
- Trenberth, K. E., and D. J. Shea, 2006: Atlantic hurricanes and natural variability in 2005. *Geophys. Res. Lett.*, **33**, L12704, doi:10.1029/2006GL026894.
- Vaganov, E. A., M. K. Hughes, A. V. Kirdyanov, F. H. Schweingruber, and P. P. Silkin, 1999: Influence of snowfall and melt timing on tree growth in subarctic Eurasia. *Nature*, **400**, 149–151.
- Walker, G. T., 1924: Correlation in seasonal variations of the weather, IX. A further study of world weather. *Indian Meteor. Mem.*, **24**, 275–332.
- Wigley, T. M. L., J. M. Lough, and P. D. Jones, 1984: Spatial patterns of precipitation in England and Wales and a revised, homogeneous England and Wales precipitation series. *J. Climatol.*, **4**, 1–25.